**Leukocyte-mimetic liposomes penetrate into tumor spheroids and suppress spheroid growth by encapsulated doxorubicin**

Tatsuya Fukuta,[1, *,#] Shintaro Yoshimi,[1,#] Kentaro Kogure[1]

[1]*Graduate School of Biomedical Sciences, Tokushima University, Shomachi 1, Tokushima, 770-8505, Japan*

[*]Corresponding author: Tatsuya Fukuta

TEL: +81-88-633-7248

FAX: +81-88-633-9572

Email: fukuta.t@tokushima-u.ac.jp

Graduate School of Biomedical Sciences, Tokushima University, Shomachi 1, Tokushima, 770-8505, Japan

[#]These authors contributed equally to this work.

**Abstract**

As leukocytes can penetrate into deep regions of a tumor mass, leukocyte-mimetic liposomes (LM-Lipo) containing leukocyte membrane proteins are also expected to penetrate into tumors by exerting properties of those membrane proteins. The aim of the present study was to examine whether LM-Lipo, which were recently demonstrated to actively pass through inflamed endothelial layers, can penetrate into tumor spheroids, and to investigate the potential of LM-Lipo for use as an anticancer drug carrier. We prepared LM-Lipo via intermembrane protein transfer from human leukemia cells; transfer of leukocyte membrane proteins onto the liposomes was determined by Western blotting. LM-Lipo demonstrated a significantly high association with human lung cancer A549 cells compared with plain liposomes, which contributed to effective anti-proliferative action by encapsulated doxorubicin hydrochloride (DOX). Confocal microscopic images showed that LM-Lipo, but not plain liposomes, could efficiently penetrate into A549 tumor spheroids. Moreover, DOX-encapsulated LM-Lipo significantly suppressed tumor spheroid growth. Thus, leukocyte membrane proteins transferred onto LM-Lipo retained their unique function, which allowed for efficient penetration of the liposomes into tumor spheroids, similar to leukocytes. In conclusion, these results suggest that LM-Lipo could be a useful tumor-penetrating drug delivery system for cancer treatment.

**Keywords**

Liposome; Leukocyte; Leukocyte-mimetic drug delivery system; Intermembrane protein transfer; Cancer; Tumor spheroid

## Introduction

Nanoparticle drug delivery systems (DDS) are broadly applied to treat various diseases, especially cancers [1,2]. Nanoparticles such as liposomes can preferentially accumulate in tumor tissue via the enhanced permeability and retention (EPR) effect that involves passive extravasation through leaky tumor blood vessels and impaired lymphatic drainage in tumors [3]. Modification of nanoparticles to allow surface display of specific ligands to target molecules, such as peptides and antibodies, is a well-known strategy to increase both accumulation of nanoparticles in tumor sites and cellular uptake by cancer cells [4-6]. However, for some cancer types, entry of nanoparticles into tumor tissue can be limited by a diminished EPR effect and by the presence of biological barriers including endothelial and stromal cells, as well as interstitial pressure in the tumor [7,8]. These obstacles can cause insufficient therapeutic efficacy of anticancer drugs delivered by nanoparticles to target tumor tissues.

To address the limitations associated with nanoparticle-mediated drug delivery into tumor tissues, circulating blood cells (e.g., red blood cells, white blood cells, and platelets) have been used as functional materials for nanoparticle preparations to develop new nanoparticle DDS that take advantage of the unique properties of these cells [7,9]. For instance, leukocytes, including monocytes and neutrophils, can associate with adhesion molecules expressed on inflamed endothelial cells, pass through the endothelial barrier, and migrate to inflammatory sites and into tumor tissue [10]. In particular, monocytes were reported to reach deep regions of the tumor and differentiate into macrophages that can make up 50% of tumor mass [11,12]. Previous reports have shown that by loading nanoparticles onto leukocytes, or by coating the surface of synthetic nanoparticles with cellular membranes, the resultant nanoparticles exhibited properties similar to those of the leukocytes and cell membranes, respectively [11,13,14]. Moreover, the resulting nanoparticles showed superior targeting ability to sites of inflammation and tumor tissues, driven largely by the functions of the cellular membrane proteins. Based on these reports, imparting leukocyte-mimetic properties to nanoparticle DDS is expected to improve delivery of cancer therapeutics using nanoparticles.

Conventional methods to reconstitute membrane proteins onto liposomes require several steps, such as solubilization and purification of cellular membrane proteins, as well as protein reconstitution with detergents, organic solvents, or sonication. However, these complicated processes can result in loss of protein activities and difficulty in regulating physicochemical properties, such as size and homogeneity; the need for improvements in these processes have recently been reported [15]. On the other hand, it was previously reported that a variety of cellular membrane proteins can be spontaneously transferred onto liposomal membranes by incubation of the cells with a liposomal suspension via a phenomenon known as intermembrane protein transfer [16]. As the transferred proteins can retain their native orientation and activities on the lipid bilayer of the harvested liposomes, intermembrane protein transfer has been used as a convenient protein reconstitution method to functionalize liposomes, as well as erythrocyte ghosts, without the need for solubilization and protein reconstitution steps [17,18]. For instance, a liposomal cancer vaccine was prepared by intermembrane protein transfer of cancer cell-derived tumor antigens onto liposomes, and this vaccine could suppress tumor growth in tumor-bearing mice [17]. By using this reconstitution method, we recently developed leukocyte-mimetic liposomes (LM-Lipo) via intermembrane protein transfer of leukocyte membrane proteins from human leukemia cells, and demonstrated that the resulting liposomes exhibited leukocyte-like functions [19]. When leukocytes pass through inflamed endothelial cells, interaction of two membrane proteins, namely lymphocyte function-associated antigen-1 (LFA-1; CD11a) and macrophage antigen-1 (Mac-1; CD11b), with intercellular adhesion molecule (ICAM)-1 was reported to be important for the mechanism of action [10,20,21]. This interaction can activate intracellular signaling pathways and transiently increase permeability of endothelial cells, resulting in leukocyte infiltration into diseased sites. By mimicking these events, we demonstrated that LM-Lipo containing both CD11a and CD11b could associate with inflamed human endothelial cells and subsequently pass through the inflamed endothelial cell layer by regulating intercellular junctions, similar to the action of leukocytes [19]. Based on this finding, we hypothesized that leukocyte-mimetic liposomes containing leukocyte membrane proteins can penetrate into a tumor

mass.

In the present study, we investigated whether LM-Lipo can penetrate into tumor tissues via the function of leukocyte membrane proteins. We first prepared LM-Lipo using intermembrane protein transfer from the human promyelocytic leukemia cell line HL-60. We then evaluated the ability of LM-Lipo to associate with cancer cells, and investigated whether LM-Lipo can penetrate into tumor tissues using a tumor spheroid model. Moreover, by encapsulating the anticancer drug doxorubicin hydrochloride (DOX) into LM-Lipo, the potential of LM-Lipo as a drug carrier for cancer therapy was investigated *in vitro*.

## Methods

### Cell cultures

The human promyelocytic leukemia cell line, HL-60, and the human Caucasian lung carcinoma cell line A549 were purchased from DS Pharma Biomedical Co., Ltd. (Osaka, Japan). HL-60 cells were cultured in RPMI-1640 medium (Nacalai Tesque, Kyoto, Japan) supplemented with 10% fetal bovine serum (FBS), 100 U/mL penicillin (Gibco, MA, USA), and 100 µg/mL streptomycin (Gibco). A549 cells were cultured in Dulbecco's modified Eagle medium (DMEM; Nacalai Tesque) supplemented with 10% FBS, 100 U/mL penicillin and 100 µg/mL streptomycin. Cells were cultured at 37ºC in a 5% $CO_2$ incubator.

### Differentiation of HL-60 cells

HL-60 cells (1.5 x $10^6$ cells/3 mL) seeded onto a 60-mm dish were incubated in RPMI-1640 medium containing 100 nM 1α, 25-dihydroxyvitamin $D_3$ ($VD_3$; Cayman Chemical, Ann Arbor, MI, USA) dissolved in dimethyl sulfoxide (DMSO) for differentiation into monocyte-like cells. The final concentration of DMSO in the media was 0.1%. For non-differentiated cells, HL-60 cells were incubated with 0.1% DMSO alone. After incubation for 48, 72, or 96 h, the cultured cells were collected and washed with phosphate-buffered saline (PBS). Then, the cells were incubated with Fc receptor blocking solution (Human TruStain FcX™; BioLegend, San Diego, CA, USA) at 4ºC for 10 min, followed by incubation with Alexa Fluor 488-conjugated anti-human CD11b antibody (BioLegend) and PE anti-human CD14 antibody (BioLegend) at 4ºC for 30 min. After washing the cells with PBS, the proportion of CD11b- and CD14-positive cells as an indication of the population of HL-60 cells that had differentiated into monocytes was determined by flow cytometry (Gallios; Beckman Coulter, CA, USA).

**Preparation of liposomes**

Egg phosphatidylcholine (EPC) and dioleoylphosphatidylethanolamine (DOPE) were purchased from NOF Corporation (Tokyo, Japan), and dicetylphosphate (DCP) was purchased from Sigma-Aldrich (Tokyo, Japan). Liposomes composed of EPC/DCP/DOPE (3.5/3/3.5 molar ratio) were prepared using the thin-film method. The abovementioned lipids dissolved in chloroform were added to test tubes and dried under nitrogen gas. To prepare fluorescence-labeled liposomes, 1, 1'-dioctadecyl-3,3,3',3'-tetramethylindocarbocyanine perchlorate ($DiIC_{18}$; Thermo Fisher Scientific, Waltham, MA, USA) dissolved in chloroform was added to the initial lipid solution at a concentration of 1 mol% total lipid. The lipid film was hydrated with 0.3 M sucrose phosphate buffer (pH 7.4) and the liposomal suspensions were then subjected to three freeze-thaw cycles in a dry-ice ethanol bath. The liposomes were sized by extrusion through polycarbonate membrane filters having 100 nm pores (Nuclepore, Cambridge, MA, USA). Finally, the particle size and ζ-potential of the liposomes were measured with a Zetasizer Nano ZS (Malvern Instruments, Worcestershire, UK).

**Intermembrane protein transfer**

After culturing HL-60 cells in the presence of 100 nM $VD_3$ or 0.1% DMSO for 72 h, the culture medium was removed by centrifugation at 1,000 *g* for 5 min at 4ºC. The cells were washed with PBS and centrifuged and the supernatant was removed. This cycle was repeated three times. Thereafter, the liposomal suspensions were added and incubated with the cells ($5.0 \times 10^6$ cells/1 mL of 1 mM liposomes) in a 35-mm dish for 60 min at 37ºC with shaking. For the control group without liposomes, the cells were incubated with 0.3 M sucrose phosphate buffer alone. The incubated liposomes and 0.3 M sucrose phosphate buffer were harvested, centrifuged at 2,000 *g* for 1 min, and the supernatants were recovered. This cycle was repeated five times to remove cells. The recovered samples were used in the following experiments.

**Observation of protein transfer onto liposomes by Western blotting**

To prepare liposome samples for SDS-PAGE, 1 mL of the recovered liposomes (1 mM) following intermembrane transfer were ultracentrifuged at 112,500 *g* for 60 min at 4ºC (Optima L-90K; Beckman Coulter, Tokyo, Japan). The pelleted liposomes were resuspended in 100 µL 0.3 M sucrose phosphate buffer to obtain a 10 mM liposome suspension. For the control group without liposomes, the incubated and recovered 0.3 M sucrose phosphate buffer was also ultracentrifuged as described above. The resulting samples (0.2 µmol lipid concentration) were exposed to 10% SDS-PAGE. For samples of HL-60 cells, cell media cultured in the presence of 100 nM $VD_3$ or 0.1% DMSO for 72 h was removed by centrifugation at 1,000 *g* for 5 min at 4ºC. The cells were washed with PBS, centrifuged, and the supernatant was subsequently removed. Then, the cells were lysed with lysis buffer (1% Triton-X100, 10 mM Tris (pH 7.5), 50 µg/mL aprotinin, 200 µM leupeptin, 2 mM phenylmethylsulfonyl fluoride, and 100 µM pepstatin A) and the protein concentration was determined with a bicinchonic acid (BCA) Protein Assay Reagent Kit (Pierce Biotechnology, Rockford, IL, USA). The resulting cellular samples (10 µg protein) were subjected to 10% SDS-PAGE. For Western blotting, anti-CD11a rabbit monoclonal antibody (ab52895; Abcam, Cambridge, UK), anti-CD11b rabbit monoclonal antibody (ab133357; Abcam), and horseradish peroxidase (HRP)-conjugated anti-rabbit IgG polyclonal antibody (A24531; Thermo Fisher Scientific, Waltham, MA,USA) were used as indicated. After performing SDS-PAGE, the proteins were electrophoretically transferred to a polyvinylidene difluoride (PVDF) membrane (Bio-Rad, Hercules, CA, USA). The PVDF membrane was incubated with 3% bovine serum albumin (BSA; Sigma-Aldrich) in Tris-HCl-buffered saline containing 0.1% Tween-20 (pH 7.4) for 1 h at 37ºC before an overnight incubation with anti-CD11a and anti-CD11b antibody at a dilution of 1:5,000 and 1:1,000, respectively, at 4ºC. The membrane was then incubated with HRP-conjugated anti-rabbit IgG polyclonal secondary antibody at a dilution of 1:2,000 for 1 h at 37ºC. After incubation with a chemiluminescent substrate reagent (ECL prime; GE Healthcare, Little Chalfont, UK), each protein was detected using a LAS-4000 mini system (Fuji Film, Tokyo, Japan).

**Liposome association assay**

A549 cells were seeded onto 35-mm glass bottom dishes at a density of 7.5 x $10^4$ cells/dish and incubated overnight. The cells were then treated with tumor necrosis factor (TNF)-α (10 ng/mL in serum-free DMEM; Fuji Film Wako Pure Chemical, Osaka, Japan) for 18 h. ICAM-1 expression was confirmed by Western blotting as described above (Section 2.5. Observation of protein transfer onto liposomes by Western blotting). Briefly, A549 cell extracts (10 μg protein) were subjected to 10% SDS-PAGE, and the proteins were transferred onto PVDF membranes, followed by reaction with anti-ICAM-1 rabbit monoclonal antibody (1:1,000; ab109361, Abcam) and anti-β-actin rabbit monoclonal antibody (ab8227; Abcam) at 4ºC overnight. Then, the membrane was incubated with the secondary antibody at a dilution of 1: 2,000 for 1 h at 37ºC, and the bands corresponding to each protein were detected.

$DiIC_{18}$ (DiI)-labeled liposomes composed of EPC/DCP/DOPE (3.5/3/3.5 molar ratio) were incubated with differentiated HL-60 cells as described above (Section 2.5). The prepared liposomes mixed in serum-free DMEM at a concentration of 0.5 mM were added to TNF-α-treated A549 cells and incubated for 3 or 24 h at 37ºC. After washing with PBS, the cells were fixed with 4% paraformaldehyde (PFA) for 10 min at 37ºC. The cells were then washed with PBS three times, and incubated with 1 μg/mL 4',6-diamidino-2-phenylindole (DAPI; Thermo Fisher Scientific) in PBS for 15 min at 37ºC. After washing with PBS, the fluorescence was observed with a confocal laser scanning microscope (LSM700, Carl Zeiss, Jena, Germany).

**Preparation of liposomes encapsulating doxorubicin**

To encapsulate doxorubicin hydrochloride (DOX; Nacalai Tesque) into liposomes, a remote-loading method using ammonium sulfate was employed. In brief, a thin lipid film composed of EPC/DCP/DOPE (3.5/3/3.5 molar ratio) was first hydrated with 250 mM ammonium sulfate. After sizing the liposomes by extrusion, the liposomal suspension was passed through a PD-10 column

(GE Healthcare Japan, Tokyo, Japan) equilibrated with PBS to remove external ammonium sulfate. The liposomes were then ultracentrifuged at 112,500 *g* for 60 min at 4ºC, and the resulting pellet was resuspended in 20 mM HEPES (pH 8.8). Then, DOX solution was added to the liposome suspension and incubated at 37ºC for 20 min. After removing unencapsulated DOX by passing through a PD-10 column, the amount of encapsulated DOX was determined by solubilizing the liposomes in 1% Triton at 65ºC for 15 min and then measuring the absorbance at 484 nm. To prepare liposomes encapsulating DOX (DOX-Lipo) that contain leukocyte membrane proteins, DOX-Lipo was incubated with differentiated HL-60 cells, and intermembrane protein transfer was performed as described above (Section 2.5).

***In vitro* cytotoxicity assay**

A549 cells were seeded (2 x $10^4$ cells/well) onto a 24-well plate and incubated overnight. The cells were then treated with TNF-α (10 ng/mL in serum-free DMEM) for 18 h. Then, DOX solution, DOX-Lipo, or DOX-Lipo incubated with differentiated HL-60 cells (LM-DOX-Lipo) was added to the cells at a final DOX concentration of 0, 0.1, 0.3 or 1 μg/mL. The cells were washed with PBS 24 h later and cultured in serum-free DMEM for an additional 24 h. Then, 48 h after the addition of each sample, the cell viability was determined using a Cell Counting Kit-8 (Dojindo, Kumamoto, Japan) in accordance with the manufacturer's instructions. The absorbance was measured using a Tecan Infinite M200 microplate reader (Tecan Japan, Kanagawa, Japan).

**Evaluation of liposomal penetration into tumor spheroids**

To prepare tumor spheroids as a model of tumor tissue, A549 cells were seeded onto Corning® 96-well spheroid plates (1.5 x $10^3$ cells/well). At 24 h after incubation, the culture medium was replaced with DMEM containing 5% FBS and 10 ng/mL TNF-α, and the cells were then cultured for 18 h. To observe liposomal distribution by confocal laser scanning microscopy, the spheroids were carefully transferred to 35-mm glass bottom dishes, and incubated with each

liposome mixed in serum-free DMEM (final lipid conc. 0.5 mM) for 24 h at 37ºC. After washing with PBS, the spheroids were fixed with 4% PFA for 10 min at 37ºC and washed with PBS. Then, the fluorescence of the liposomes in the spheroids was assessed by confocal laser scanning microscopy. For quantitative evaluation of liposomal penetration into the spheroids, the depth of DiI fluorescence from the spheroid surface was measured using image analysis software (NIH ImageJ). The liposome depth at 4 arbitrary sites within each spheroid was measured. Average penetration depths were calculated across 8 spheroids for each experiment. Four independent experiments were performed.

**Anticancer efficacy of leukocyte-mimetic DOX-Lipo in tumor spheroids**

A549 cells were seeded onto Corning® 96-well spheroid plates ($1.5 \times 10^3$ cells/well). At 30 h after seeding, the medium was replaced with DMEM containing 5% FBS and 10 ng/mL TNF-α, and the cells were then cultured for 18 h. At 48 h after the initial seeding, DOX solution, DOX-Lipo, or LM-DOX-Lipo was added to the spheroids at a final concentration of 50 μg/mL in serum-free DMEM, and incubated for 24 h. After removal of each sample, fresh 10% FBS DMEM was added and replaced every other day. Spheroid morphology was observed with a fluorescence microscope (Axio Vert.A1, Carl Zeiss) for 4 days, and images were acquired. Spheroid volume was calculated using the following equation: $0.5 \times a \times b^2$ (where a and b represent the largest and smallest diameter, respectively). Spheroid diameters were measured from the microscopic images using image analysis software (NIH ImageJ).

**Statistical analysis**

Statistical differences were evaluated by one-way analysis of variance (ANOVA) with the Tukey *post-hoc* test. Differences between 2 groups were determined using Student's *t*-test. Data are presented as mean ± standard deviation (S.D.).

## Results

### Differentiation of HL-60 cells into monocyte-like cells

In this study, we used HL-60 cells as the donor for leukocyte membrane proteins, since treatment of these cells with 1α, 25-dihydroxyvitamin $D_3$ ($VD_3$) can induce differentiation into monocyte-like cells that express leukocyte membrane proteins such as CD11a and CD11b, which are related to leukocyte adhesion to cancer cells [22,23]. Differentiation of HL-60 cells into monocyte-like cells by $VD_3$ treatment was evaluated by flow cytometry with the monocyte markers CD11b and CD14 used as indicators of differentiation, as reported previously [24]. Cultivation of HL-60 cells with 100 nM $VD_3$ remarkably increased the population of CD11b- and CD14-positive cells, namely differentiated monocyte-like cells, 48, 72, and 96 h after treatment (Fig. 1A). On the other hand, few CD11b- and CD14-positive cells were observed in the absence of $VD_3$ treatment. The proportion of CD11b- and CD14-positive cells was approximately 70% at 72 h after initiating $VD_3$ treatment, and remained unchanged at 96 h (Fig. 1B), indicating that HL-60 cells were mostly differentiated into monocyte-like cells upon treatment with $VD_3$ for 72 h. Based on these results, we used HL-60 cells treated with $VD_3$ for 72 h (as monocyte-differentiated HL-60 cells) as the donor of leukocyte membrane proteins in subsequent experiments.

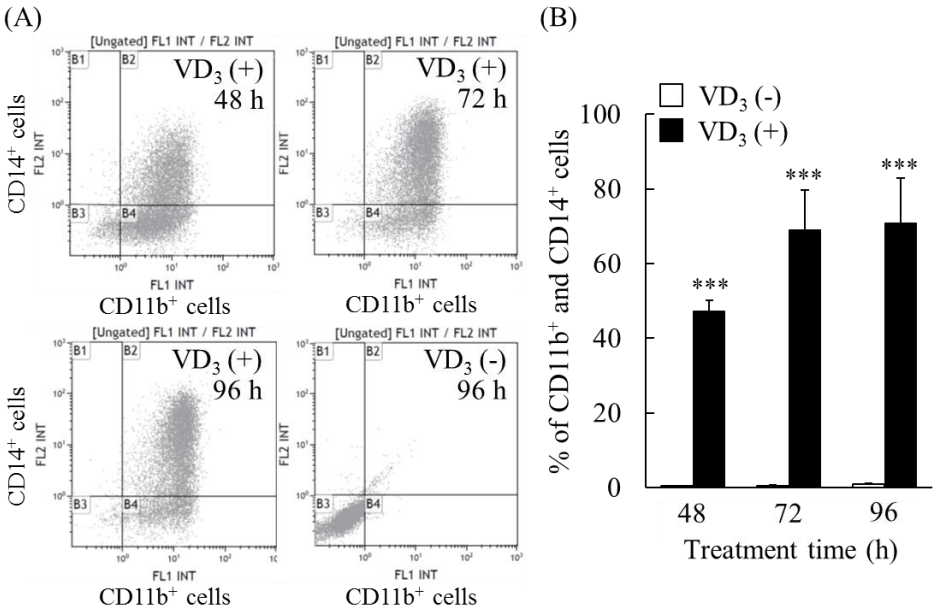

Figure 1. Differentiation of HL-60 cells into monocyte-like cells by $VD_3$ treatment.

(A) HL-60 cells were treated with 100 nM $VD_3$ for 48, 72, or 96 h to induce differentiation into monocyte-like cells. For the non-differentiated group, cells were cultured in the presence of 0.1% DMSO. After incubation for the indicated time, the cells were harvested and stained with Alexa Fluor 488-conjugated anti-CD11b antibody and PE anti-CD14 antibody. The proportion of CD11b and CD14-positive cells was then measured by flow cytometry. (B) Percentage of CD11b and CD14-positive cells determined from the histograms. The data show the mean ± S.D. (n=3). Significant difference: *** $P<0.001$ vs. $VD_3$ (-).

**Intermembrane protein transfer of leukocyte membrane proteins onto liposomes**

We investigated intermembrane protein transfer of leukocyte membrane proteins onto liposomes using both differentiated and non-differentiated cells. Results of our previous studies demonstrated that incorporation of the amphiphilic anionic compound DCP into liposomes induces phase separation in the liposomal membrane, which results in an increase in protein transfer efficiency [25,26]. Moreover, in our recent report on the development of LM-Lipo, we prepared liposomes composed of EPC (containing unsaturated phospholipids) and those composed of dimyristoylphosphatidylcholine (DMPC; saturated phospholipid), and examined the effect of incorporation of DCP and a fusogenic phospholipid, DOPE, into each liposome on the protein transfer efficiency, by determining the amount of transferred proteins using a BCA assay and Western blotting [19]. Among the liposomes used in the study, the transfer efficiency of membrane proteins, particularly CD11a and CD11b, was highest for liposomes composed of EPC/DCP/DOPE (3.5/3/3.5 molar ratio). Moreover, compared with LM-Lipo composed of DMPC/DCP/DOPE (3.5/3/3.5 molar ratio), LM-Lipo composed of EPC/DCP/DOPE (3.5/3/3.5 molar ratio) were found to highly associate with inflamed endothelial cells. Therefore, in the present study, we used liposomes composed of EPC/DCP/DOPE (3.5/3/3.5 molar ratio) for preparation of LM-Lipo. The particle size, polydispersity index (PDI), and ζ-potential of the liposomes are shown in Table 1. As CD11a and CD11b (and not CD14) are involved in leukocyte adhesion to cancer cells, transfer of CD11a and CD11b onto liposomes was representatively observed using Western blotting. Results confirmed the presence of

CD11a in liposomes incubated with both HL-60 cells (Fig. 2A). CD11b transfer was observed only for liposomes incubated with $VD_3$-treated monocyte-differentiated cells (Fig. 2B). Meanwhile, neither CD11a nor CD11b was detected in cells incubated only with 0.3 M sucrose phosphate buffer. These results confirmed successful intermembrane protein transfer of leukocyte membrane proteins onto liposomes, consistent with our previous report [19]. Although we could not determine the loading amount of CD11a and CD11b onto liposomes, we estimated the transfer efficiency of those proteins using the BCA assay, silver staining, and Western blotting in our previous report [19]. Results showed the transfer efficiencies of CD11a and CD11b from HL-60 cells onto liposomes to be 0.07% and 0.2% of the total amount of cellular protein, respectively (the total amount of cellular protein employed for intermembrane protein transfer in this study was determined to be 594.4 ± 28.8 μg; hence, loading amounts of CD11a and CD11b onto liposomes were estimated to be 416.2 ± 20.2 ng and 1188.9 ± 57.6 ng, respectively). In subsequent experiments, liposomes prepared with differentiated HL-60 cells are referenced as leukocyte-mimetic liposomes (LM-Lipo). As shown in Table 1, after intermembrane protein transfer, the average particle size of the liposomes was significantly increased by approximately 30 nm ($P$<0.05; Table 1). The ζ-potential of the liposomes was essentially unaffected by the membrane protein transfer.

Table 1. Physicochemical properties of liposomes

| | Size (d.nm) | PDI | ζ-Potential (mV) |
|---|---|---|---|
| Liposomes | 114.2 ± 13.2 | 0.261 ± 0.07 | -10.8 ± 1.5 |
| LM-Lipo | 142.3 ± 7.14 | 0.323 ± 0.03 | -12.8 ± 1.34 |

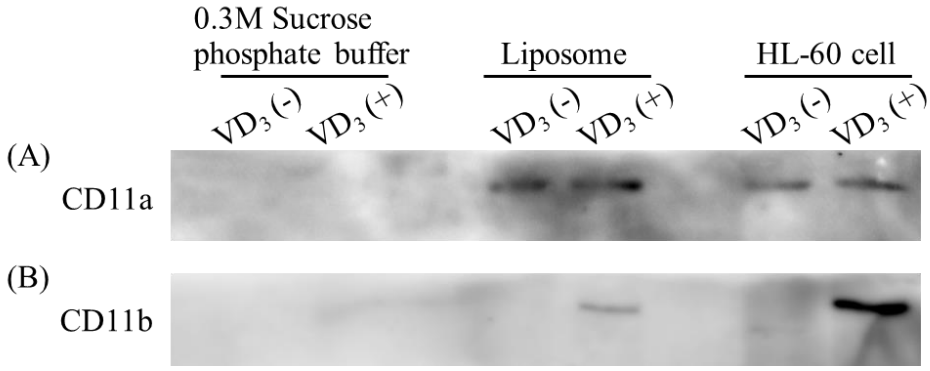


Figure 2. Leukocyte membrane protein transfer onto liposomes via intermembrane protein transfer from HL-60 cells.

(A, B) Liposomes composed of EPC/DCP/DOPE (3.5/3/3.5 molar ratio) or 0.3 M sucrose phosphate buffer were incubated with non-differentiated ($VD_3$ (-)) or differentiated ($VD_3$ (+)) HL-60 cells for 60 min. Each lane indicates liposomal samples (0.2 μmol as total lipid), samples prepared without liposomes (0.3 M sucrose phosphate buffer), and cell extracts of non-differentiated or differentiated HL-60 cells (10 μg protein) subjected to SDS-PAGE. Western blotting was performed to observe transfer of CD11a (A) and CD11b (B) onto the liposomes. The detected molecular weights of CD11a and CD11b are approximately 180 kDa and 170 kDa, respectively, consistent with the product datasheet. The leftmost lane indicates the bands for the Western Protein Standard (MagicMark™ XP; Thermo Fisher Scientific).

**Association of leukocyte-mimetic liposomes with cancer cells**

Association of LM-Lipo with the human cancer cell line A549 was next evaluated. Prior to liposome treatment, A549 cells were treated with the inflammatory cytokine TNF-α for 18 h to mimic the inflammatory tumor microenvironment [27,28]. We used Western blotting to confirm that treatment of A549 cells with TNF-α induced expression of ICAM-1 (Fig. 3A), which is known to interact with both CD11a and CD11b [10,20]. We investigated the association of DiI-labeled LM-Lipo with TNF-α treated A549 cells 3 and 24 h after treatment, and observed fluorescence with a confocal laser scanning microscope. The confocal images showed that at 3 h after treatment with liposomes, DiI fluorescence in A549 cells treated with LM-Lipo was more intense than that for cells treated with plain liposomes (Fig. 3B). Quantitative data analyzed with ImageJ similarly indicated significantly higher fluorescence intensity for the LM-Lipo-treated cells compared to cells treated with plain

liposomes (Fig. 3C). Higher fluorescence was observed in each liposome-treated group at 24 h after treatment compared with 3 h after treatment, and LM-Lipo were found to more strongly associate with A549 cells than plain liposomes (Figs. 3D and E). These results suggest that the functions of leukocyte membrane proteins are retained following transfer of the proteins onto liposomal membranes, and that liposomes can achieve leukocyte-mimetic properties that promote their subsequent association with cancer cells.

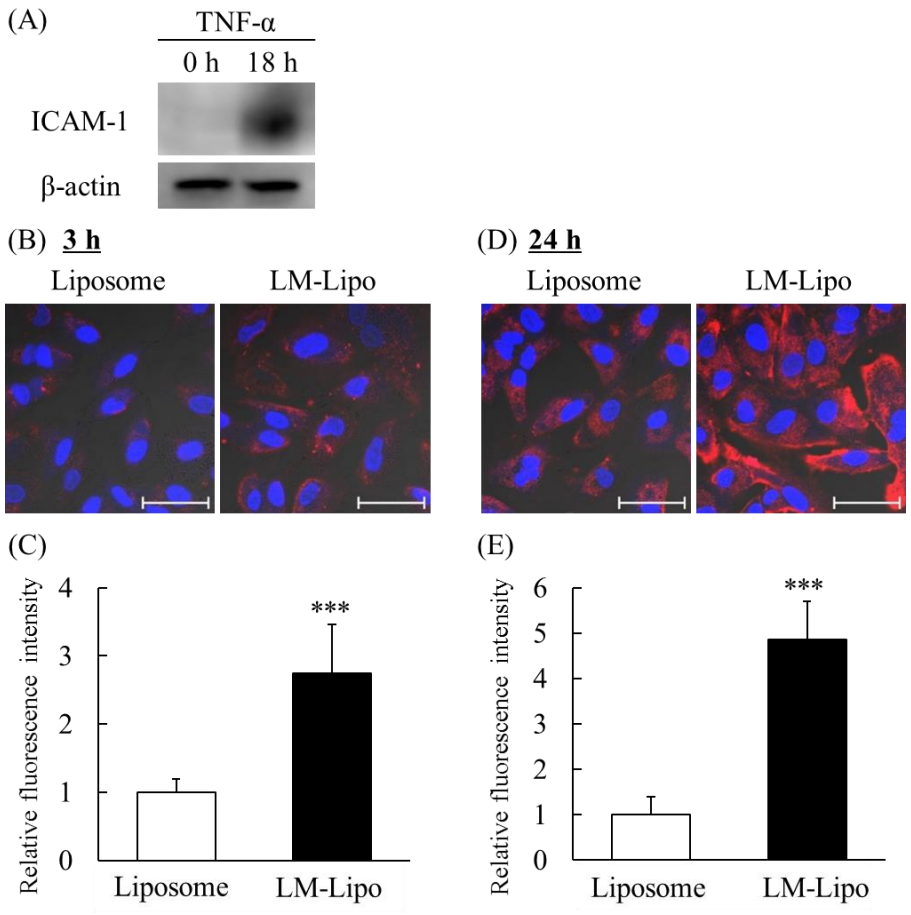


Figure 3. Association of leukocyte-mimetic liposomes with A549 cells.

A549 cells were treated with TNF-α (10 ng/mL) for 18 h, and DiI-labeled liposomes or LM-Lipo were then added. (A) Expression of ICAM-1 in TNF-α-treated A549 cells confirmed by Western blotting. At 3 (B, C) or 24 h (D, E) after incubation, the cells were fixed and the nuclei were counterstained with DAPI. Fluorescence images were then obtained by confocal laser scanning microscopy. Merged images of DiI (liposome; red) and DAPI (nucleus; blue) are shown. Scale bars = 50 μm. (C, E) The relative fluorescence intensities of DiI to those for the groups treated with plain liposomes were calculated from at least 8 images per group of A549 cells for each experiment using the Image J software. The data show the mean ± S.D. ($n \geq 8$). Significant difference: *** $P<0.001$ vs. Liposome. Three independent experiments were performed, and all produced similar profiles.

**Cancer cell growth inhibition by treatment with LM-Lipo encapsulating DOX**

We next prepared liposomes encapsulating the anticancer drug DOX and evaluated the anti-proliferative effect of LM-DOX-Lipo against A549 cells to demonstrate the potential of LM-Lipo as a drug delivery carrier. The particle size, PDI and ζ-potential of each liposome were shown in Table. 2. Following intermembrane protein transfer, the particle size of LM-DOX-Lipo was significantly ~50 nm larger than unmodified plain DOX-Lipo, similar to that seen for LM-Lipo (Table 1). LM-DOX-Lipo significantly inhibited the proliferation of A549 cells compared with DOX-Lipo at each DOX concentration (Fig. 4). These results suggest that higher association of LM-Lipo with human lung cancer A549 cells could result in its superior anticancer effect compared with plain liposomes.

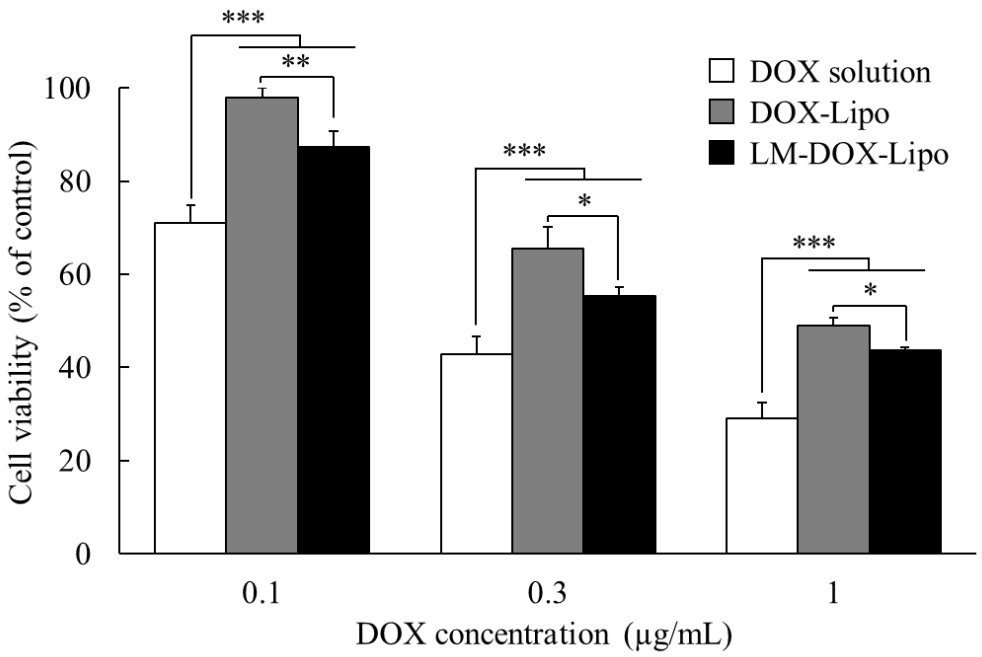


Figure 4. Anti-proliferative effect of LM-DOX-Lipo against A549 cancer cells.

A549 cells were treated with DOX solution (white bar), DOX-Lipo (gray bar), or LM-DOX-Lipo (black bar) at DOX doses of 0.1, 0.3, 1 μg/mL for 24 h. After washing with PBS, the cells were cultured for another 24 h. Cell viability was determined by a WST-8 assay. The data show the mean ± S.D. (n=6). Significant differences: * $P<0.05$, ** $P<0.01$, and *** $P<0.001$.

**Table 2. Physicochemical properties of DOX-encapsulated liposomes**

| | Size (d.nm) | PDI | ζ-Potential (mV) |
|---|---|---|---|
| DOX-Lipo | 153.9 ± 12.3 | 0.304 ± 0.03 | -15.1 ± 0.86 |
| LM-DOX-Lipo | 203.5 ± 12.0 | 0.423 ± 0.05 | -14.4 ± 2.0 |

**Evaluation of tumor penetration of LM-Lipo in an A549 spheroid model**

To examine tumor penetration capability of LM-Lipo *in vitro*, a tumor spheroid model was prepared using A549 cells. Spheroid models are reported to display properties that are similar to those of tumor mass, and thus are recognized as a more useful model to evaluate cellular uptake and cytotoxic effect of candidate drugs than 2D-cultured cells [29]. TNF-α-treated A549 spheroids were treated with DiI-labeled plain liposomes or DiI-labeled LM-Lipo for 24 h. The distribution of each liposome in the spheroids was then observed by confocal laser scanning microscopy and Z-stack images for each group were acquired. In the plain liposome-treated group, DiI fluorescence was detected in the margins of the spheroid, but little penetration of the liposomes into the spheroid was observed (Fig. 5A). However, in the LM-Lipo-treated group, significant DiI fluorescence was observed at the margins, as well as the interior of the spheroids (Fig. 5B), indicating that LM-Lipo penetrates into the A549 tumor spheroids. Quantitative analysis of liposomal penetration into A549 tumor spheroids was performed by measuring the depth of the liposomes from the spheroid surface in confocal images. Results also showed a significantly higher ability of LM-Lipo to penetrate the spheroids compared with plain liposomes (Fig. 5C).

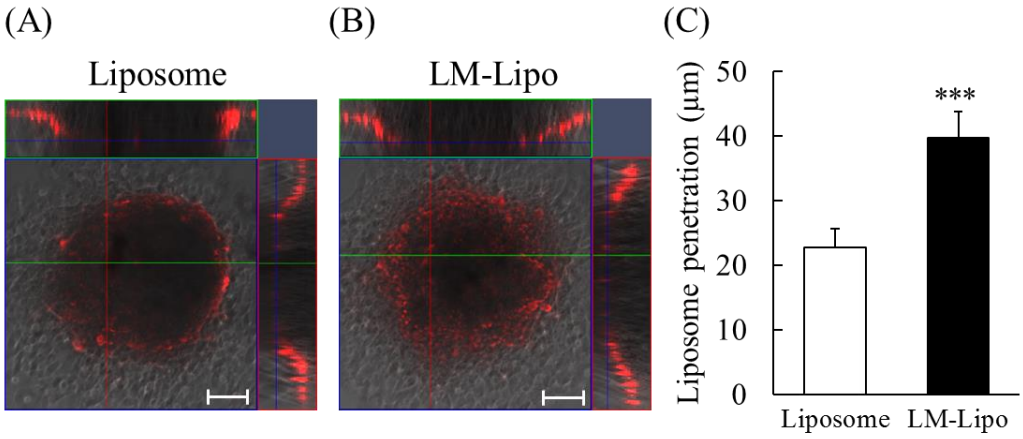


Figure 5. Penetration of LM-Lipo into A549 tumor spheroids.

A549 tumor spheroids were treated with DiI-labeled liposomes or DiI-labeled LM-Lipo for 24 h. After washing with PBS, DiI fluorescence in the spheroids was observed by confocal laser scanning microscopy. Z-stack images of spheroids treated with (A) DiI-labeled liposomes and (B) DiI-labeled LM-Lipo. Scale bars = 50 μm. (C) Quantitative analysis of the depth of liposomal penetration from the spheroid surface. Liposomal depth was measured at 4 arbitrary sites per spheroid; average penetration depths were calculated across 8 spheroids for each experiment. Four independent experiments were performed. The data show the mean ± S.D. (n=4). Significant differences: *** $P<0.001$.

**Anticancer effect of LM-DOX-Lipo in an A549 spheroid model**

Finally, the anticancer efficacy of LM-Lipo encapsulating DOX was assessed in the A549 tumor spheroid model. The size of the tumor spheroids gradually increased in the non-treated control group over 4 days (Fig. 6A). Treatment with DOX solution or DOX-Lipo at a DOX concentration of 50 μg/mL suppressed the growth of tumor spheroids (Fig. 6A). Notably, treatment of the spheroids with LM-DOX-Lipo also markedly decreased the size of the spheroids. The tumor volume was calculated from the images using ImageJ, and the anticancer effect was evaluated. Tumor volume in the DOX solution and DOX-Lipo groups tended to decrease over the 4 days, whereas that of the non-treated group gradually increased (Fig. 6B). On the other hand, treatment with LM-DOX-Lipo decreased the tumor volume and showed a significantly higher anticancer effect than DOX-Lipo. The effects of empty liposomes and empty LM-Lipo without DOX on the growth of tumor spheroids were also examined. Results showed that tumor spheroid growth was not suppressed by treatment

with empty liposomes or empty LM-Lipo, indicating that the anti-cancer effects of DOX-Lipo and LM-DOX-Lipo were due to encapsulated DOX (Supplementary Figure 1).

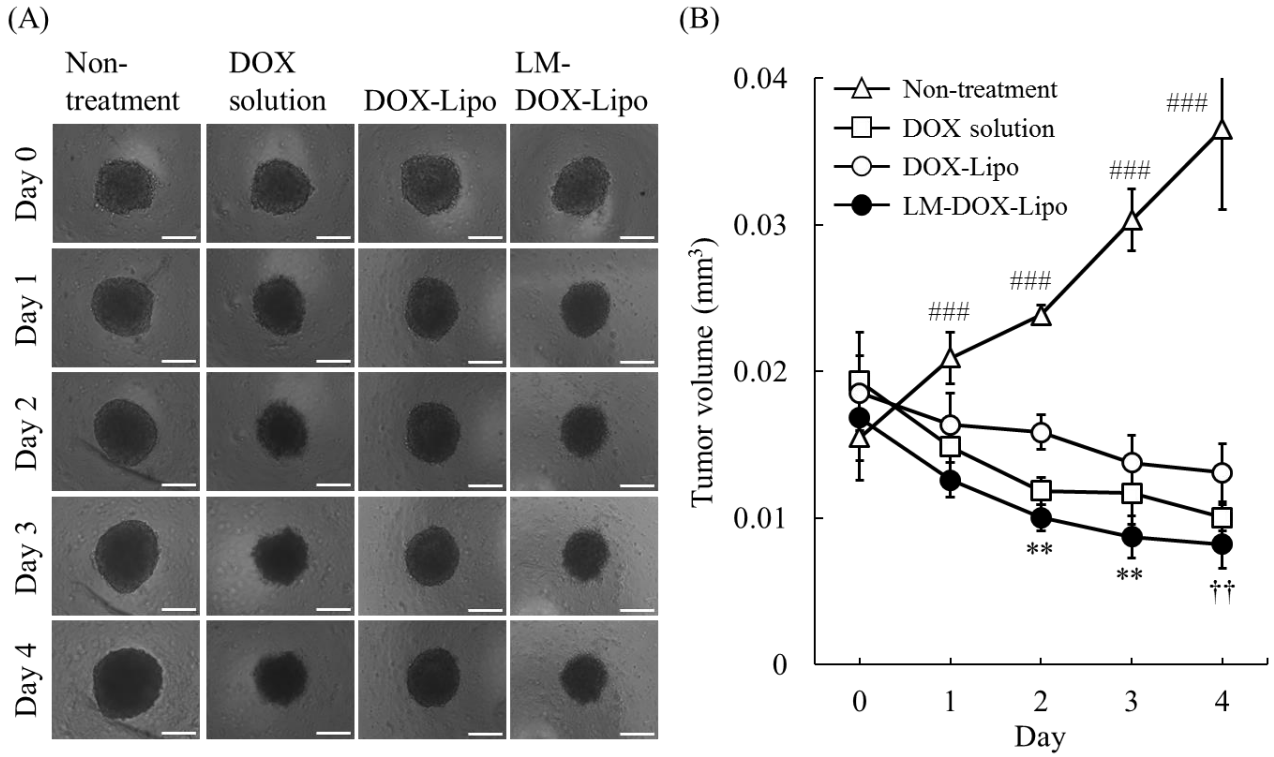


Figure 6. Anticancer effect of LM-DOX-Lipo in an A549 tumor spheroid model.

DOX solution, DOX-Lipo or LM-DOX-Lipo at DOX doses of 50 μg/mL was added to A549 tumor spheroids, and incubated for 24 h. (A) Optical images of spheroids acquired over 4 days after the initiation of DOX treatment. Scale bars = 200 μm. (B) Growth profiles of A549 spheroids generated by calculating spheroid volume. The data show the mean ± S.D. (n=8). Significant differences: ** $P<0.01$ vs. DOX solution and DOX-Lipo for the LM-DOX-Lipo group, †† $P<0.01$ vs. DOX-Lipo for LM-DOX-Lipo group, and $^{###}$ $P<0.001$ vs. other groups for the non-treatment group.

## Discussion

As passive delivery of anticancer drugs into tumor tissues is often hampered by the presence of biological barriers such as inflamed tumor vessels and tumor mass, nanoparticles that can actively pass through inflamed vessels and penetrate into the tumor tissue are needed [7,8]. To overcome these challenges, application of the unique properties of leukocytes to DDS has received considerable attention, as leukocytes can pass through inflamed endothelial cells and penetrate into deep regions of tumor tissues [30,31]. In our previous study, we demonstrated that LM-Lipo containing the leukocyte membrane proteins CD11a and CD11b that were transferred from human leukemia HL-60 cells onto liposomal membranes by intermembrane protein transfer could pass through the inflamed endothelial cell layer via induction of a decrease in vascular-endothelial cadherin expression [19]. Based on these findings, we hypothesized that LM-Lipo could also penetrate into tumor tissues, in addition to inflamed endothelial cells, by utilizing the function of leukocyte membrane proteins.

Using differentiated monocyte-like and non-differentiated HL-60 cells, we first examined transfer of leukocyte membrane proteins onto liposomal membranes. Differentiation of HL-60 cells into monocyte-like cells by treatment with $VD_3$ was confirmed by monitoring expression of CD11b and CD14 (Fig. 1). For intermembrane protein transfer, we used liposomes composed of EPC/DCP/DOPE (3.5/3/3.5 molar ratio) since incorporation of the amphiphilic anionic compound DCP and the fusogenic lipid DOPE was shown to increase transfer efficiency of membrane proteins [19,25]. Western blotting results showed that the leukocyte membrane proteins CD11a and CD11b were successfully transferred onto liposomes following incubation with $VD_3$-treated differentiated HL-60 cells (Fig. 2). In addition, liposome particle size after incubation was significantly increased by ~30 nm compared with plain liposomes (Table 1). This increase in size is likely associated with the incorporation of leukocyte membrane proteins onto liposomal membranes. These results indicated that liposomes possessing leukocyte membrane proteins, termed LM-Lipo, were successfully prepared by intermembrane protein transfer from differentiated HL-60 cells, similar to our previous report [19].

Next, we investigated the function of LM-Lipo using 2D-cultured A549 cells treated with TNF-α to mimic an inflammatory tumor microenvironment and induce expression of ICAM-1 (Fig. 3A). Confocal microscopy showed that LM-Lipo had significantly higher association with TNF-α-treated A549 cells compared to cells treated with plain liposomes (Fig. 3). Since both plain liposomes and LM-Lipo had negative ζ-potentials, association of those liposomes with cancer cells via electrostatic interactions was unlikely. Nevertheless, LM-Lipo did efficiently associate with A549 cells, implying that the interaction was mediated by leukocyte membrane proteins that retained native activity after transfer onto liposomes. We also evaluated the anti-proliferative effects of both plain and LM-Lipo encapsulating the anti-cancer drug DOX; treatment with LM-DOX-Lipo showed significantly greater cytotoxic effects compared with plain DOX-Lipo at each DOX concentration (Fig. 4). This higher cytotoxic activity is likely due to the more efficient association of LM-DOX-Lipo mediated by the leukocyte membrane proteins; released DOX from liposomes and DOX taken up with LM-Lipo both exert anticancer effects. Moreover, it was confirmed that transfer of leukocyte membrane proteins onto liposomes occurred regardless of DOX encapsulation.

Tumor spheroid models are reported to reflect the characteristics of a tumor mass, and thus spheroids are considered to be a more suitable cell culture system to investigate the efficacy of candidate anticancer drugs [29,32]. Here we used the A549 tumor spheroid model to demonstrate the usefulness of LM-Lipo as a tumor-targeting DDS by evaluating liposome penetration into the spheroids. Z-stack images obtained by confocal laser scanning microscopy showed that LM-Lipo, but not plain liposomes, could penetrate into tumor spheroids (Fig. 5). Of note, even though the average particle size of LM-Lipo (142.3 ± 7.14 nm) was ~30 nm larger than plain liposomes (114.2 ± 13.2 nm; Table 1), penetration of LM-Lipo into the tumor spheroid was nonetheless observed. These results imply that the function of leukocyte membrane proteins incorporated onto the liposomes contributed to the capability of LM-Lipo to penetrate the tumor spheroids. Further, although treatment with the DOX solution and plain DOX-Lipo exerted an anti-proliferative effect on A549 spheroids, treatment with LM-DOX-Lipo successfully promoted spheroid regression (Fig. 6). On the

other hand, tumor spheroid growth was not suppressed by treatment with empty liposomes or empty LM-Lipo (Supplementary Figure 1). Notably, LM-DOX-Lipo had substantial penetration of tumor spheroids despite having a significantly larger particle size (~50 nm larger than plain liposomes; Table 2). These results suggest that LM-Lipo efficiently penetrated into tumor spheroids via functional incorporated membrane proteins, and that both the DOX released from liposomes and DOX taken up with the liposomes could effectively exert a pharmacological effect that resulted in regression of tumor spheroid growth.

The size of nanoparticles was previously reported to be important for penetration into tumor mass, and smaller particles (e.g., 30 nm) were shown to be suitable for penetration into deep regions of tumors [33]. However, in this study, LM-Lipo that were over 100 nm in diameter could still penetrate the tumor spheroids due to the presence of functional leukocyte membrane proteins. These findings suggest that imparting leukocyte-mimetic properties to liposomes via intermembrane protein transfer could be a promising strategy to develop tumor-targeting DDS capable of penetrating into a tumor mass. Although a detailed mechanism for the increase in size of LM-DOX-Lipo relative to DOX-Lipo is not clear, the average particle size of LM-Lipo (142.3± 7.14 nm) was significantly larger than that of plain liposomes (114.2 ± 13.2 nm) following transfer of membrane proteins onto the liposomes (Table 1). DOX encapsulation also increased the average size of plain liposomes. These results suggest that both transfer of membrane proteins onto liposomes and DOX encapsulation might affect the state of liposomal membranes, resulting in an increase in the particle size of LM-DOX-Lipo compared with DOX-Lipo.

To further demonstrate the usefulness of LM-Lipo, *in vivo* experiments using tumor-bearing mice are needed. As the lipid composition of LM-Lipo contains an anionic compound, namely DCP, the ζ-potential of LM-Lipo exhibited a negative charge (Tables 1 and 2). This negative surface charge is thought to contribute to a reduction in the interaction of systemically injected LM-Lipo with proteins in the bloodstream, and to prevent recognition by macrophages. In fact, our previous study demonstrated that systemically injected negatively-charged liposomes encapsulating an anti-cancer

drug can be delivered to tumor tissues in tumor-bearing mice, resulting in successful suppression of tumor growth [34]. It was also reported that integration of leukocyte membrane proteins onto nanoparticles can prolong circulation time in the bloodstream via reduction of non-specific recognition by immune cells [35]. Hence, it is expected that the negatively charged liposomal surface and the leukocyte membrane proteins of LM-Lipo might be conducive for stable circulation in the bloodstream and subsequent accumulation in tumor tissues.

Modification of the nanoparticle surface with polyethylene glycol (PEG) is generally employed to prolong circulation time via formation of a hydrophilic layer on the surface of the nanoparticles. However, for preparation of LM-Lipo via intermembrane protein transfer, liposomal modification with PEG should prevent transfer of membrane proteins by inhibiting contact of the liposomal membrane with the donor cells. If PEG modification of LM-Lipo is required for future *in vivo* application, insertion of PEG-lipid derivatives onto the liposomes after intermembrane protein transfer would be suitable to avoid a decrease in the protein transfer efficiency. On the other hand, modification of LM-Lipo with an excess of PEG is thought to reduce the function of leukocyte membrane proteins and decrease their targeting abilities. Hence, it is necessary to optimize the amount of PEG on LM-Lipo to allow PEG-modified LM-Lipo to exert the function of leukocyte membrane proteins while retaining the ability for prolonged circulation.

In the present study, liposomes attained leukocyte-mimetic properties following intermembrane protein transfer from differentiated HL-60 cells without loss of activity of the transferred membrane proteins, and LM-Lipo could penetrate into tumor spheroids, similar to that seen for leukocytes that can infiltrate tumors [12,36]. Our recent study also demonstrated that LM-Lipo possessing both CD11a and CD11b could efficiently pass through ICAM-1 expressing inflamed endothelial cell layers [19]. Considering systemic delivery of anticancer drugs into tumor tissues *in vivo*, nanoparticles that can both penetrate into tumor mass and pass through inflamed tumor vessels are preferable, since the low degree of the EPR effect is an issue associated with cancer therapy using nanoparticles [7,8]. The results of this study suggest that LM-Lipo could be a useful DDS that can

overcome limitations of nanoparticle-based cancer therapy, including those accompanying the EPR effect and the presence of biological barriers, to be an effective DDS to treat cancers.

**Acknowledgement**

This research was funded by a Grant-in-Aid for Scientific Research from the Japan Society for the Promotion of Science (JSPS, grant number 17H06906 and 19K16336). The authors gratefully acknowledge support from the Research Program for the Development of Intelligent Tokushima Artificial Exosome (iTEX) from Tokushima University.

**References**

1. Oku N 2017. Innovations in liposomal DDS technology and its application for the treatment of various diseases. Biol Pharm Bull 40(2):119-127.

2. Torchilin VP 2014. Multifunctional, stimuli-sensitive nanoparticulate systems for drug delivery. Nat Rev Drug Discov 13(11):813-827.

3. Maeda H, Nakamura H, Fang J 2013. The EPR effect for macromolecular drug delivery to solid tumors: Improvement of tumor uptake, lowering of systemic toxicity, and distinct tumor imaging in vivo. Adv Drug Deliv Rev 65(1):71-79.

4. Allen TM 2002. Ligand-targeted therapeutics in anticancer therapy. Nat Rev Cancer 2(10):750-763.

5. Danhier F, Feron O, Preat V 2010. To exploit the tumor microenvironment: Passive and active tumor targeting of nanocarriers for anti-cancer drug delivery. J Control Release 148(2):135-146.

6. Fukuta T, Asai T, Kiyokawa Y, Nakada T, Bessyo-Hirashima K, Fukaya N, Hyodo K, Takase K, Kikuchi H, Oku N 2017. Targeted delivery of anticancer drugs to tumor vessels by use of

liposomes modified with a peptide identified by phage biopanning with human endothelial progenitor cells. Int J Pharm 524(1-2):364-372.

7. Anselmo AC, Mitragotri S 2014. Cell-mediated delivery of nanoparticles: taking advantage of circulatory cells to target nanoparticles. J Control Release 190:531-541.

8. Blanco E, Shen H, Ferrari M 2015. Principles of nanoparticle design for overcoming biological barriers to drug delivery. Nat Biotechnol 33(9):941-951.

9. Luk BT, Zhang L 2015. Cell membrane-camouflaged nanoparticles for drug delivery. J Control Release 220(Pt B):600-607.

10. Vestweber D 2015. How leukocytes cross the vascular endothelium. Nat Rev Immunol 15(11):692-704.

11. Anselmo AC, Gilbert JB, Kumar S, Gupta V, Cohen RE, Rubner MF, Mitragotri S 2015. Monocyte-mediated delivery of polymeric backpacks to inflamed tissues: a generalized strategy to deliver drugs to treat inflammation. J Control Release 199:29-36.

12. Murdoch C, Giannoudis A, Lewis CE 2004. Mechanisms regulating the recruitment of macrophages into hypoxic areas of tumors and other ischemic tissues. Blood 104(8):2224-2234.

13. Parodi A, Quattrocchi N, van de Ven AL, Chiappini C, Evangelopoulos M, Martinez JO, Brown BS, Khaled SZ, Yazdi IK, Enzo MV, Isenhart L, Ferrari M, Tasciotti E 2013. Synthetic nanoparticles functionalized with biomimetic leukocyte membranes possess cell-like functions. Nat Nanotechnol 8(1):61-68.

14. Palomba R, Parodi A, Evangelopoulos M, Acciardo S, Corbo C, de Rosa E, Yazdi IK, Scaria S, Molinaro R, Furman NE, You J, Ferrari M, Salvatore F, Tasciotti E 2016. Biomimetic carriers mimicking leukocyte plasma membrane to increase tumor vasculature permeability. Sci Rep 6:34422.

15. Molinaro R, Corbo C, Martinez JO, Taraballi F, Evangelopoulos M, Minardi S, Yazdi IK, Zhao P, De Rosa E, Sherman MB, De Vita A, Toledano Furman NE, Wang X, Parodi A, Tasciotti E 2016. Biomimetic proteolipid vesicles for targeting inflamed tissues. Nat Mater 15(9):1037-1046.

16. Huestis WH, Newton A 1986. Intermembrane protein transfer. Band 3, the erythrocyte anion transporter, transfers in native orientation from human red blood cells into the bilayer of phospholipid vesicles. J Biol Chem 261(34):16274-16278.

17. Shibata R, Noguchi T, Sato T, Akiyoshi K, Sunamoto J, Shiku H, Nakayama E 1991. Induction of in vitro and in vivo anti‐tumor responses by sensitization of mice with liposomes containing a crude butanol extract of leukemia cells and transferred inter‐membranously with cell‐surface proteins. Int J Cancer 48(3):434-442.

18. Kogure K, Itoh T, Okuda O, Hayashi K, Ueno M 2000. The delivery of protein into living cells by use of membrane fusible erythrocyte ghosts. Int J Pharm 210(1-2):117-120.

19. Fukuta T, Yoshimi S, Tanaka T, Kogure K 2019. Leukocyte-mimetic liposomes possessing leukocyte membrane proteins pass through inflamed endothelial cell layer by regulating intercellular junctions. Int J Pharm 563:314-323.

20. Smith C, Marlin S, Rothlein R, Toman C, Anderson D 1989. Cooperative interactions of LFA-1 and Mac-1 with intercellular adhesion molecule-1 in facilitating adherence and transendothelial migration of human neutrophils in vitro. J Clin Invest 83(6):2008-2017.

21. Etienne-Manneville S, Manneville JB, Adamson P, Wilbourn B, Greenwood J, Couraud PO 2000. ICAM-1-coupled cytoskeletal rearrangements and transendothelial lymphocyte migration involve intracellular calcium signaling in brain endothelial cell lines. J Immunol 165(6):3375-3383.

22. Drayson MT, Michell RH, Durham J, Brown G 2001. Cell proliferation and CD11b expression are controlled independently during HL60 cell differentiation initiated by 1,25 alpha-dihydroxyvitamin D(3) or all-trans-retinoic acid. Exp Cell Res 266(1):126-134.

23. Ji Y, Studzinski GP 2004. Retinoblastoma protein and CCAAT/enhancer-binding protein β are required for 1, 25-dihydroxyvitamin D3-induced monocytic differentiation of HL60 cells. Cancer Res 64(1):370-377.

24. White SL, Belov L, Barber N, Hodgkin PD, Christopherson RI 2005. Immunophenotypic changes induced on human HL60 leukaemia cells by 1alpha,25-dihydroxyvitamin D3 and

12-O-tetradecanoyl phorbol-13-acetate. Leuk Res 29(10):1141-1151.

25. Kogure K, Okuda O, Nakamura C, Hayashi K, Ueno M 1999. Effects of Incorporation of Various Amphiphiles into Recipient Liposome Membraneson Inter-Membrane Protein Transfer. Chem Pharm Bull 47(8):1117-1120.

26. Kogure K, Nakamura C, Okuda O, Hayashi K, Ueno M 1997. Effect of dicetylphosphate or stearic acid on spontaneous transfer of protein from influenza virus-infected cells to dimyristoylphosphatidylcholine liposomes. Biochim Biophys Acta Biomembr 1329(1):174-182.

27. Heinrich EL, Walser TC, Krysan K, Liclican EL, Grant JL, Rodriguez NL, Dubinett SM 2012. The inflammatory tumor microenvironment, epithelial mesenchymal transition and lung carcinogenesis. Cancer Microenviron 5(1):5-18.

28. Salvatore V, Teti G, Focaroli S, Mazzotti MC, Mazzotti A, Falconi M 2017. The tumor microenvironment promotes cancer progression and cell migration. Oncotarget 8(6):9608.

29. LaBarbera DV, Reid BG, Yoo BH 2012. The multicellular tumor spheroid model for high-throughput cancer drug discovery. Exp Opin Drug Discov 7(9):819-830.

30. Chu D, Gao J, Wang Z 2015. Neutrophil-mediated delivery of therapeutic nanoparticles across blood vessel barrier for treatment of inflammation and infection. ACS Nano 9(12):11800-11811.

31. Kang T, Zhu Q, Wei D, Feng J, Yao J, Jiang T, Song Q, Wei X, Chen H, Gao X, Chen J 2017. Nanoparticles Coated with Neutrophil Membranes Can Effectively Treat Cancer Metastasis. ACS Nano 11(2):1397-1411.

32. Pampaloni F, Reynaud EG, Stelzer EH 2007. The third dimension bridges the gap between cell culture and live tissue. Nat Rev Mol Cell Biol 8(10):839-845.

33. Nishiyama N, Matsumura Y, Kataoka K 2016. Development of polymeric micelles for targeting intractable cancers. Cancer Sci 107(7):867-874.

34. Hama S, Utsumi S, Fukuda Y, Nakayama K, Okamura Y, Tsuchiya H, Fukuzawa K, Harashima H, Kogure K 2012. Development of a novel drug delivery system consisting of an

antitumor agent tocopheryl succinate. J Control Release 161(3):843-851.

35. Corbo C, Molinaro R, Taraballi F, Toledano Furman NE, Hartman KA, Sherman MB, De Rosa E, Kirui DK, Salvatore F, Tasciotti E 2017. Unveiling the in Vivo Protein Corona of Circulating Leukocyte-like Carriers. ACS Nano 11(3):3262-3273.

36. Kolaczkowska E, Kubes P 2013. Neutrophil recruitment and function in health and inflammation. Nat Rev Immunol 13(3):159-175.

**Figure legends**

Figure 1. Differentiation of HL-60 cells into monocyte-like cells by $VD_3$ treatment.

(A) HL-60 cells were treated with 100 nM $VD_3$ for 48, 72, or 96 h to induce differentiation into monocyte-like cells. For the non-differentiated group, cells were cultured in the presence of 0.1% DMSO. After incubation for the indicated time, the cells were harvested and stained with Alexa Fluor 488-conjugated anti-CD11b antibody and PE anti-CD14 antibody. The proportion of CD11b and CD14-positive cells was then measured by flow cytometry. (B) Percentage of CD11b and CD14-positive cells determined from the histograms. The data show the mean ± S.D. (n=3). Significant difference: *** $P<0.001$ vs. $VD_3$ (-).

Figure 2. Leukocyte membrane protein transfer onto liposomes via intermembrane protein transfer from HL-60 cells.

(A, B) Liposomes composed of EPC/DCP/DOPE (3.5/3/3.5 molar ratio) or 0.3 M sucrose phosphate buffer were incubated with non-differentiated ($VD_3$ (-)) or differentiated ($VD_3$ (+)) HL-60 cells for 60 min. Each lane indicates liposomal samples (0.2 μmol as total lipid), samples prepared without liposomes (0.3 M sucrose phosphate buffer), and cell extracts of non-differentiated or differentiated HL-60 cells (10 μg protein) subjected to SDS-PAGE. Western blotting was performed to observe transfer of CD11a (A) and CD11b (B) onto the liposomes. The detected molecular weights of CD11a and CD11b are approximately 180 kDa and 170 kDa, respectively, consistent with the product datasheet. The leftmost lane indicates the bands for the Western Protein Standard (MagicMark™ XP; Thermo Fisher Scientific).

Figure 3. Association of leukocyte-mimetic liposomes with A549 cells.

A549 cells were treated with TNF-α (10 ng/mL) for 18 h, and DiI-labeled liposomes or LM-Lipo were then added. (A) Expression of ICAM-1 in TNF-α-treated A549 cells confirmed by

Western blotting. At 3 (B, C) or 24 h (D, E) after incubation, the cells were fixed and the nuclei were counterstained with DAPI. Fluorescence images were then obtained by confocal laser scanning microscopy. Merged images of DiI (liposome; red) and DAPI (nucleus; blue) are shown. Scale bars = 50 μm. (C, E) The relative fluorescence intensities of DiI to those for the groups treated with plain liposomes were calculated from at least 8 images per group of A549 cells for each experiment using the Image J software. The data show the mean ± S.D. (n≥8). Significant difference: *** $P<0.001$ vs. Liposome. Three independent experiments were performed, and all produced similar profiles.

Figure 4. Anti-proliferative effect of LM-DOX-Lipo against A549 cancer cells.

A549 cells were treated with DOX solution (white bar), DOX-Lipo (gray bar), or LM-DOX-Lipo (black bar) at DOX doses of 0.1, 0.3, 1 μg/mL for 24 h. After washing with PBS, the cells were cultured for another 24 h. Cell viability was determined by a WST-8 assay. The data show the mean ± S.D. (n=6). Significant differences: * $P<0.05$, ** $P<0.01$, and *** $P<0.001$.

Figure 5. Penetration of LM-Lipo into A549 tumor spheroids.

A549 tumor spheroids were treated with DiI-labeled liposomes or DiI-labeled LM-Lipo for 24 h. After washing with PBS, DiI fluorescence in the spheroids was observed by confocal laser scanning microscopy. Z-stack images of spheroids treated with (A) DiI-labeled liposomes and (B) DiI-labeled LM-Lipo. Scale bars = 50 μm. (C) Quantitative analysis of the depth of liposomal penetration from the spheroid surface. Liposomal depth was measured at 4 arbitrary sites per spheroid; average penetration depths were calculated across 8 spheroids for each experiment. Four independent experiments were performed. The data show the mean ± S.D. (n=4). Significant differences: *** $P<0.001$.

Figure 6. Anticancer effect of LM-DOX-Lipo in an A549 tumor spheroid model.

DOX solution, DOX-Lipo or LM-DOX-Lipo at DOX doses of 50 μg/mL was added to A549

tumor spheroids, and incubated for 24 h. (A) Optical images of spheroids acquired over 4 days after the initiation of DOX treatment. Scale bars = 200 μm. (B) Growth profiles of A549 spheroids generated by calculating spheroid volume. The data show the mean ± S.D. (n=8). Significant differences: ** $P<0.01$ vs. DOX solution and DOX-Lipo for the LM-DOX-Lipo group, †† $P<0.01$ vs. DOX-Lipo for LM-DOX-Lipo group, and $^{\#\#\#}$ $P<0.001$ vs. other groups for the non-treatment group.

Supplementary Fig. 1. Effect of empty liposomes and LM-Lipo on tumor spheroid growth.

Empty liposomes composed of EPC/DCP/DOPE (3.5/3/3.5 molar ratio) or LM-Lipo mixed in serum-free DMEM at a total lipid concentration of 0.5 mM were added to A549 tumor spheroids and incubated for 24 h. (A) Optical images of tumor spheroids acquired over 4 days after the start of liposomal treatment. Scale bars = 200 μm. (B) Growth profiles of A549 tumor spheroids generated by calculating spheroid volume. The data show the mean ± S.D. (n=8).